Role of endocytosis in sonoporation-mediated membrane permeabilization and uptake of small molecules: a electron microscopy study

Physical Biology

PAPER

Role of endocytosis in sonoporation-mediated membrane permeabilization and uptake of small molecules: a electron microscopy study

A Zeghimi[1], **J M Escoffre**[1] **and A Bouakaz**

Inserm UMR 930, Université François-Rabelais de Tours, 10 bd Tonnellé, F-37032 Tours, Cedex 1, France
[1] AZ and JME have contributed equally to this work.

E-mail: jean-michel.escoffre@univ-tours.fr **and** ayache.bouakaz@univ-tours.fr

Keywords: sonoporation, membrane permeabilization, endocytosis, small molecules, electron microscopy

OPEN ACCESS

RECEIVED
27 June 2015

REVISED
12 August 2015

ACCEPTED FOR PUBLICATION
1 September 2015

PUBLISHED
23 November 2015

Abstract

Sonoporation is a physical method that has been successfully used to deliver drugs into living cells both *in vitro* and *in vivo* for experimental and therapeutic purposes. Despite numerous studies on this topic, often reporting successful outcomes, very little is known about the mechanisms involved in the hypothesized membrane permeabilization processes. In this study, electron microscopy was used to investigate the ultra-structural modifications of cell membranes, induced by sonoporation. Here, we demonstrate that sonoporation in the presence of microbubbles induces the formation of a significant number of transient and permeant structures at the membrane level. These structures were transient with a half-life of 10 min and had a heterogeneous size distribution ranging from a few nanometers to 150 nm. We demonstrated that the number and the size of these structures were positively correlated with the enhanced intracellular uptake of small molecules. In addition, we showed that these structures were associated with caveolae-dependent endocytosis for two thirds of the recorded events, with the remaining one third related to non-specific routes such as membrane disruptions as well as caveolae-independent endocytosis. In conclusion, our observations provide direct evidences of the involvement of caveolae-endocytosis in cell membrane permeabilization to small molecules after sonoporation.

1. Introduction

The biomedical applications of therapeutic molecules are limited because their physico-chemical properties impose inefficient transmembrane transport abilities and/or the deficiencies of membrane transport mechanisms. To overcome these limitations, the development of efficient targeted delivery methods has been developed to increase the local concentration of therapeutic molecules at the desired site while minimizing side effects to healthy tissues.

Sonoporation, based on the use of high frequency ultrasound (1–10 MHz) in combination with gas microbubbles was introduced as a non-viral physical method that is currently under evaluation for gene and drug delivery [1, 2]. Sonoporation involves the treatment of a desired volume of cells *in vitro* or tissue *in vivo* with ultrasound in the presence of microbubbles. These microbubbles, which are formulated as lipid, albumin or polymer shelled micrometer sized gas bodies in aqueous suspension, are commonly mixed with cells for *in vitro* applications or administered by intravascular/intratissue injection for *in vivo* applications [3]. The exposure of microbubbles to ultrasound causes their periodic oscillations and/or their collapse, under appropriate insonation conditions. It is now known that these oscillations can induce micro-streaming, shock waves and/or micro-jets that can affect the integrity of biological barriers (e.g., cell membrane, endothelial barrier) [4–6]. The use of sonoporation to deliver therapeutic molecules to tissues has been extensively explored over the past decade. For example, the loco-regional delivery of anti-tumoral drugs has been reported [7, 8] and is now under clinical investigation [9]. Sonoporation has been successfully used to transfer nucleic acids into the heart, skeletal muscle, tumors, vessels, liver and kidney [3]. This method enables exogenous delivery of

molecules with minimal cell or tissue damage, inflammation and/or immunological response. In addition, ultrasound can be non-invasively targeted to a specific volume of superficial tissues or deeply embedded organs. Taken together, these properties make sonoporation an innovative and compelling method for gene and drug delivery [3, 10].

Although sonoporation shows promise in a variety of research disciplines and clinical applications, very little is known about the molecular and cellular processes that underlie the transfer of exogenous molecules across the plasma membrane to the cytoplasm where their intracellular targets occur [11]. Based on indirect evidences [12, 13], the formation of membrane pores and the stimulation of endocytosis pathways have both been hypothesized as main mechanisms in the sonoporation process. Indeed, by assessing the uptake or release of molecular markers [12, 14] and by measuring ionic conductivities [15, 16], previous studies have shown that sonoporation induces a transient increase in membrane permeability through likely the generation of transient membrane pores and the stimulation of endocytosis. The membrane pores might facilitate the intracellular delivery of small molecules (<4 kDa) while the endocytosis might induce the uptake of macromolecules (>4 kDa). Recent developments in electron microscopy offer new opportunities for the monitoring and identification of the membrane structures involved in the transmembrane delivery of exogenous molecules. Using scanning electron microscopy (SEM), Mehier-Humbert *et al* first reported the visualization of few 100 nm sized pores, but their size distribution could not be defined, neither the duration of their occurrence [13]. A subsequent study estimated the size of these pores to be of the order 0.001–4.31 μm [17]. However, membrane pores with sizes >400 nm have been associated with a significant loss of cell viability [18]. A common feature of almost all previous studies is that they are all based on a simple visualization of dark and spherically-shaped structures across the cell surface immediately after sonoporation. Although these structures have been classified as pores, there has been no correlation between the presence of these structures and the increased transmembrane permeabilization of non-permeant molecules, neither with the viability of cells. In addition, there has been no direct study on the transient character of sonoporation and on the number and the fate of these structures in the minutes and hours after sonoporation.

To gain direct insights into membrane modifications and explore the cellular membrane response, which follow sonoporation, we made sequential recordings of the major transient phase after ultrasound exposure in presence of microbubbles on human glioblastoma cells using electron microscopy. Sonoporation effects were followed by ultra-structural analysis of cell membrane modifications. Overall consistency of these results was assessed through a comparison with the results of SYTOX-Green uptake (i.e. a small and non-permeant molecule) obtained using flow cytometry. All these results are here discussed taking into account the existing knowledge about the mechanisms of membrane sonoporation.

2. Material and methods

2.1. Cell culture

Human U-87 MG glioblastoma cells were derived from a malignant glioma (European Collection of Cell Cultures, Salisbury, UK). These cells were grown as a monolayer in OptiMEM® High W/GlutaMAX-I (Life Technologies Corp., Carlsbad, CA) supplemented with 10% fetal calf serum (FCS) (PAA Laboratories, Veliz-Villacoublay, France). The cells were routinely subcultured every 4 days and incubated at 37 °C in a humidified atmosphere in a 5% CO_2 incubator. This cancer cell line is commonly used to develop and optimize sonoporation for the delivery of chemotherapeutic drugs and nucleic acids [19–21].

2.2. Endocytosis inhibition

U-87 MG cells were pre-treated with 50 μM genistein (Sigma-Aldrich, St. Louis, MO) at 37 °C for 1 h to inhibit caveolae-mediated endocytosis. Immunofluorescence and MTT assays demonstrated that this treatment condition led to efficient and non-toxic effect of genistein for U-87 MG (unpublished data). Genistein hampers caveolae-coated vesicle internalization by hindering dynamin-2 ring assembly, which is crucial for late stages of membrane invagination [22, 23].

2.3. Membrane permeabilization

Membrane permeabilization was monitored by assessing the intracellular uptake of SYTOX-Green intercalating fluorescent dye (Life Technologies Corp.), using flow cytometry [14]. This low molecular weight molecule (600 Da) is a non-permeant fluorescent dye used as model drug and exhibits a 100- to 1000-fold increase in fluorescence intensity upon binding to nucleic acid.

As previously described, U-87 MG cells were seeded on 18 mm diameter cover slips placed in 24 well plates. Cells were cultured in OptiMEM® High W/GlutaMAX-I supplemented with 10% FCS, to 80% confluence at 37 °C in a humidified atmosphere with 5% CO_2 incubator. Four experimental groups were defined: (i) control (i.e., untreated), (ii) US alone (i.e., without microbubbles), (iii) US + MB (i.e., sonoporation) and (iv) genistein and US+MB (i.e., genistein pretreatment followed by sonoporation). Briefly, cell culture medium was replaced with OptiMEM® High W/GlutaMAX-I supplemented with 1% FCS. To minimize the generation of standing waves [24], the 24-well plates were placed on top of a platform and partially immersed within a deionized and degassed

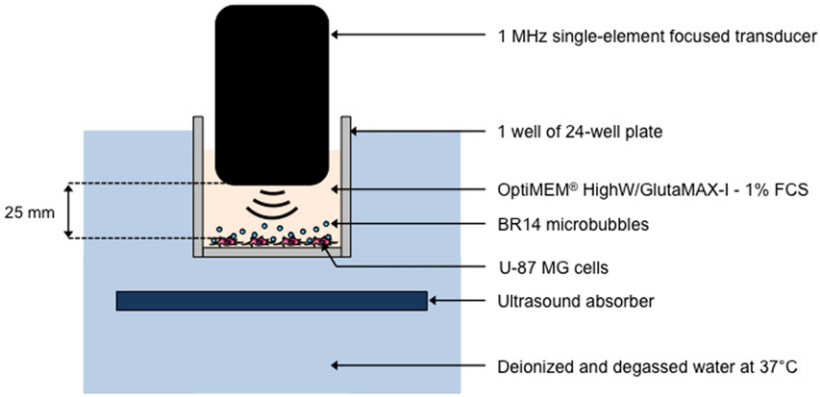

Figure 1. Experimental setup for *in vitro* sonoporation (drawing not to scale).

Table 1. Experimental groups and applied ultrasound settings.

Conditions	Intensity (W cm^{-2})	Duty cycle (%)	Exposure time (s)	Microbubbles
A	—	—	—	−
B	1	20	60	−
C	0.5	20	60	+
D	1	20	60	+
E	1	20	10	+
F	1	10	60	+
G	2	50	60	+

water tank at 37 °C with ultrasound-absorbing rubber pad placed underneath (figure 1). SYTOX-Green and/or BR-14 microbubbles (Bracco Research Geneva, Switzerland) were added immediately before ultrasound application to give a final concentration of 1 μM SYTOX-Green and a microbubble-to-cell ratio of 5 (i.e., optimal microbubble concentration to prevent cell detachment upon ultrasound exposure). A 1 MHz single-element focused transducer with a diameter of 15 mm and focused at 25 mm (Vevo SoniGene™ system, VisualSonics BV, Netherlands) was immersed into each well of 24-well plates (figure 1). The focal distance between the front face of transducer and the cell monolayer was kept constant with a transducer holder. Various exposure conditions were investigated by varying, either the duty cycle (10%, 20% and 40%), the acoustic intensity (0.5–2 W cm^{-2}), or the total exposure time (10 or 60 s) (see table 1).

Both the permeabilization level (i.e., percentage of SYTOX-Green positive cells, which describes the level of permeabilized cells) and efficiency (i.e., mean fluorescence intensity associated to percentage of SYTOX-Green positive cells, which describes indirectly the intracellular amount of SYTOX-Green) were assessed by flow cytometry, at different time points (i.e., 0, 5, 10, 15, 30, 60 min) after sonoporation. Cells were harvested by trypsinization and resuspended in complete medium. The cell suspension was centrifuged (3 min, 800 g) and was then re-suspended in phosphate saline buffer. The cells were then stained with propidium iodide at 0.5 μg mL^{-1} in order to quantify the cell mortality. Fluorescence histograms were recorded by using a flow cytometry (Beckman Coulter Inc., Fullerton, CA) and analyzed using the Kaluza software supplied by the manufacturer. A minimum of 10 000 events was analyzed to generate each histogram. The gate was arbitrary set for the detection of green and red fluorescence intensities. The permeabilization level and efficiency were determined from the population of viable cells.

2.4. Electron microscopic assessment and analysis

Using the same set-up and procedure previously described for membrane permeabilization (table 1), ultra-structural modifications of cell plasma membrane were assessed, in the absence of SYTOX-Green, both by scanning (SEM) and transmission electron microscopy (TEM). Briefly, cells were fixed by incubating in 4% paraformaldehyde and 1% glutaraldehyde in 0.1 M phosphate buffer (pH 7.2) for 48 h. SEM specimens were dehydrated in a graded series of ethanolic solution (50%–100%) and critical point dried in liquid carbon dioxide. SEM imaging was achieved by first, attaching the coverslips with fixed adherent cells to sample stubs and sputter coating with platinum (5 nm) followed by imaging with a LEO DSM 982 SEM (Zeiss, Germany). In contrast, TEM specimens were post-fixed by incubating in 2% osmium tetroxide solution (Electron Microscopy Science, Hatfield, PA) for 1 h. They were then dehydrated by immersion in a graded series of ethanolic solutions (50%–100%), cleared in propylene oxide, and embedded in Epon resin (Sigma-Aldrich), which was allowed to polymerize for 48 h at 60 °C. Seriated ultrathin sections (70 nm) were cut with a Leica Ultracut UCT ultramicrotome, placed on electron microscopy one-slot grids coated with Formvar film and stained with 5% uranyl acetate for 20 min and 5% lead citrate. The serial sections were then imaged at 100 kV with a JOEL 1011 Transmission electron microscope (JEOL Ltd, Tokyo, Japan) connected to a

Gatan digital camera driven by Digital Micrograph software (Gatan, Pleasanton, CA) for image acquisition and analysis. Images were retrospectively reviewed by an expert independent reader blinded to treatment assignment. The number of transient permeant structures, endocytic events and membrane disruptions were determined for each image (10 images/cell; $N > 30$ cells/experimental condition).

2.5. Statistical analysis

Data were presented as mean ± standard error of the mean (SEM) of five independent experiments and analyzed for statistical significance by Statistical analysis was executed using the non-parametric Mann-Whitney U test (StatPlus:mac, Analyst Soft Inc., Alexandria, VA). Significance was defined as $p < 0.05$ (NS, non-significance, $^{*}p < 0.05$, $^{**}p < 0.01$ and $^{***}p < 0.001$).

3. Results and discussion

3.1. Sonoporation enhances SYTOX-Green uptake through the formation of permeant structures

To directly monitor membrane modifications induced by sonoporation, U-87 MG glioblastoma cells were exposed to different ultrasound conditions (table 1) in the presence of the small and non-permeant molecule, SYTOX-Green, either with (condition A, C–G) or without BR-14 microbubbles (condition B). The ultrasound exposure of cells in the absence of microbubbles (condition B) was characterized by 28 ± 1% of permeabilized cells as compared to 59 ± 2% cells ($p < 0.05$) for ultrasound combined with microbubbles (condition D, figure 2(A)). Significantly, sonoporation exhibited a eight-fold increase in cell permeabilization efficiency i.e., 105 ± 3 in arbitrary units (a.u.) as compared to 13 ± 3 a.u. for ultrasound alone ($p < 0.001$) (figure 2(B)).

Under these acoustic parameters, the presence of microbubbles significantly affected the cell viability (6 ± 1% versus 2 ± 1%; $p < 0.05$) (figure 2(C)). In addition, the ultrasound conditions C, E and F were less efficient to permeabilize cells compared to the condition D (figure 2). Under the ultrasound condition G, the permeabilization level (99 ± 1%) and efficiency (222 ± 2 a.u.) were significantly increased compared to the condition D ($p < 0.05$). However, this condition dramatically increased the cell mortality (40 ± 1%; $p < 0.05$). Altogether, these results suggested that the acoustic parameters of the condition D were the most appropriate to get a high percentage of permeabilized and viable cells.

To visualize ultra-structural modification of cell membranes induced by sonoporation, cells were immediately fixed after sonoporation and analyzed using SEM. SEM images of control (untreated) U-87 MG glioblastoma cells (figure 3(A), condition A) were characterized by a smooth surface with sparse distribution of microvilli. Under the control condition, one sees no membrane disruptions, which could be construed as due to putative artifactual effect of specimen fixation procedure. Compared to US alone condition (figure 3(A), condition B), the combination of US + MB induce the formation of dark and spherically-shaped structures in addition to scattered patches that were randomly distributed across cell membranes (figure 3(A), conditions C–G), suggesting a direct involvement of sonoporation in the creation of these structures. Apart from condition G, one can notice that the high permeabilization level and efficiency shown in figure 2(B) were positively associated to a high mean number of observed structures per cell (figure 3(B)). For this reason, these structures are hereafter termed *permeant structures*. The size distribution of the observed structures was heterogeneous with a diameter ranging from a few nanometers up to 150 nm (figure 3(C)), irrespective of the ultrasound conditions tested in this study. These finding are in good agreement with previous data that highlighted a relationship between molecular size and intracellular delivery efficiency [17, 25]. Indeed, sonoporation was more efficient for the intracellular delivery of small molecules (i.e., anticancer drugs) when compared to macromolecules (i.e., plasmid DNA) [12, 13]. Under the ultrasound condition G, the mean number of *permeant structures* per cells was low but the size of these structures (0.5–4 μm) was much higher than those induced in other ultrasound conditions (figure 3(C)). In agreement with previous publications [18], the formation of such micro-sized structures (also known as membrane wounds) are associated with loss of cell viability as confirmed by the quantification of cell viability displayed in figure 2(C). It was noticeable that the count of the *permeant structures* was significantly higher for sonoporation in the presence of microbubbles (633 ± 32 structures) as compared to ultrasound alone (189 ± 39 structures, $p < 0.001$; figure 2(B)). These results suggest that microbubble-assisted ultrasound treatment led to a higher number of *permeant structures* and increased cell permeabilization level compared with ultrasound treatment alone, thus suggesting that microbubbles potentiated the ultrasound-mediated membrane permeabilization [25, 26].

3.2. Permeant membrane structures are transient

To investigate the temporal evolution of sonoporation-induced *permeant structures*, cells were fixed at increasingly later time-intervals (i.e., 0, 5, 10, 15, 30 and 60 min after sonoporation) after sonoporation and both the count (number of *permeant structure*/cell) and size (projected diameter) of *permeant structures* were quantified (figure 4). Figures 4(A) and (B) show both a progressive and significant decrease in the number and size of the *permeant structures* towards

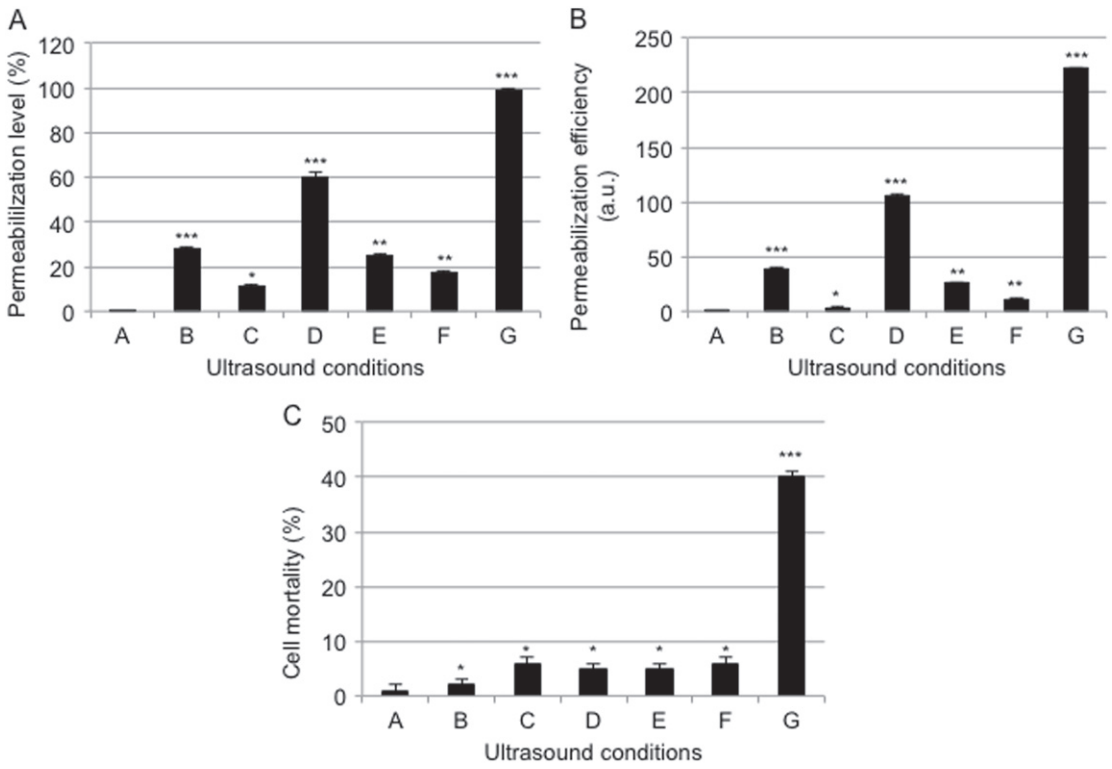

Figure 2. Effect of sonoporation using various ultrasound excitation parameters on the cell permeabilization and viability. U-87 MG cells were incubated with SYTOX-Green with or without microbubbles and then insonated under different conditions (table 1). Permeabilization level (A) and efficiency were monitored immediately after sonoporation by flow cytometry. The cell viability (C) was assessed by propidium iodide staining. Data expressed as mean ± SD was calculated from three independent experiments. Statistical analysis was performing using the non-parametric Mann-Whitney test. Significance was defined as $p < 0.05$ (NS, non-significance, $^{*}p < 0.05$, $^{**}p < 0.01$ and $^{***}p < 0.001$ compared to the condition (A).

later time-intervals, and show that membrane resealing commenced <5 min after sonoporation. The kinetics of membrane resealing, i.e., the number of *permeant structures* as a function of time after sonoporation, was characterized by exponential decay with a half-life close to 10 min (figure 4(C)). One hour after sonoporation, most cells exhibited a fully recovered and intact membrane clearly showing that they had recovered their native membrane integrity (figure 4(A)) [27–29]. The duration of membrane recovery was shown to range from a few seconds to a maximum of a few hours, with differing kinetics, depending on the ultrasound parameters, the marker size and the cell physiology [11, 30].

Moreover, we evaluated whether there was any association between membrane recovery and cellular uptake of SYTOX-Green. The permeabilization level and efficiency were measured when this molecule was added to the cell medium at increasingly later time-intervals after sonoporation. Analysis of membrane recovery by SEM images and by SYTOX-Green uptake (figure 4(D)) showed a strong and significant positive correlation (Pearson's coefficient, 0.98; $p < 0.05$). These results demonstrate that the *permeant structures* were transient and their number correlated positively with the uptake of small molecules. In the rest of the present study, these structures will be termed *transient and permeant structures* (TPSs).

The membrane surface of these resealed cells was characterized by a high number of scattered patches (figure 4(A)) that were not observed in the control cells (figure 3(A)). The size of these patches was larger than the TPS sizes. One hour after sonoporation, few patches were observed on the membrane surface of cells, which recovered their membrane integrity, thus demonstrating again the transient nature of these structures (figure 4(A)). These scattered patches indicate that the membrane resealing process is probably more complicated than a simple self-rearrangement of plasma membrane. In agreement with previous studies [17, 31], these results support the model of a patching mechanism as membrane repair process. Sonoporation has been shown to trigger calcium ion influx through the permeabilized membrane [31], which might then cause the translocation of intracellular vesicles towards the permeabilized membrane and rapidly fuse together and also with the adjacent plasma membrane [17].

3.3. Caveolae-dependent endocytosis is involved in sonoporation-mediated membrane permeabilization

To further characterize these TPSs, the cells were immediately fixed after sonoporation and embedded. TEM was used to examine the plasma membrane of thin-sectioned cells. As shown in figure 5(A),

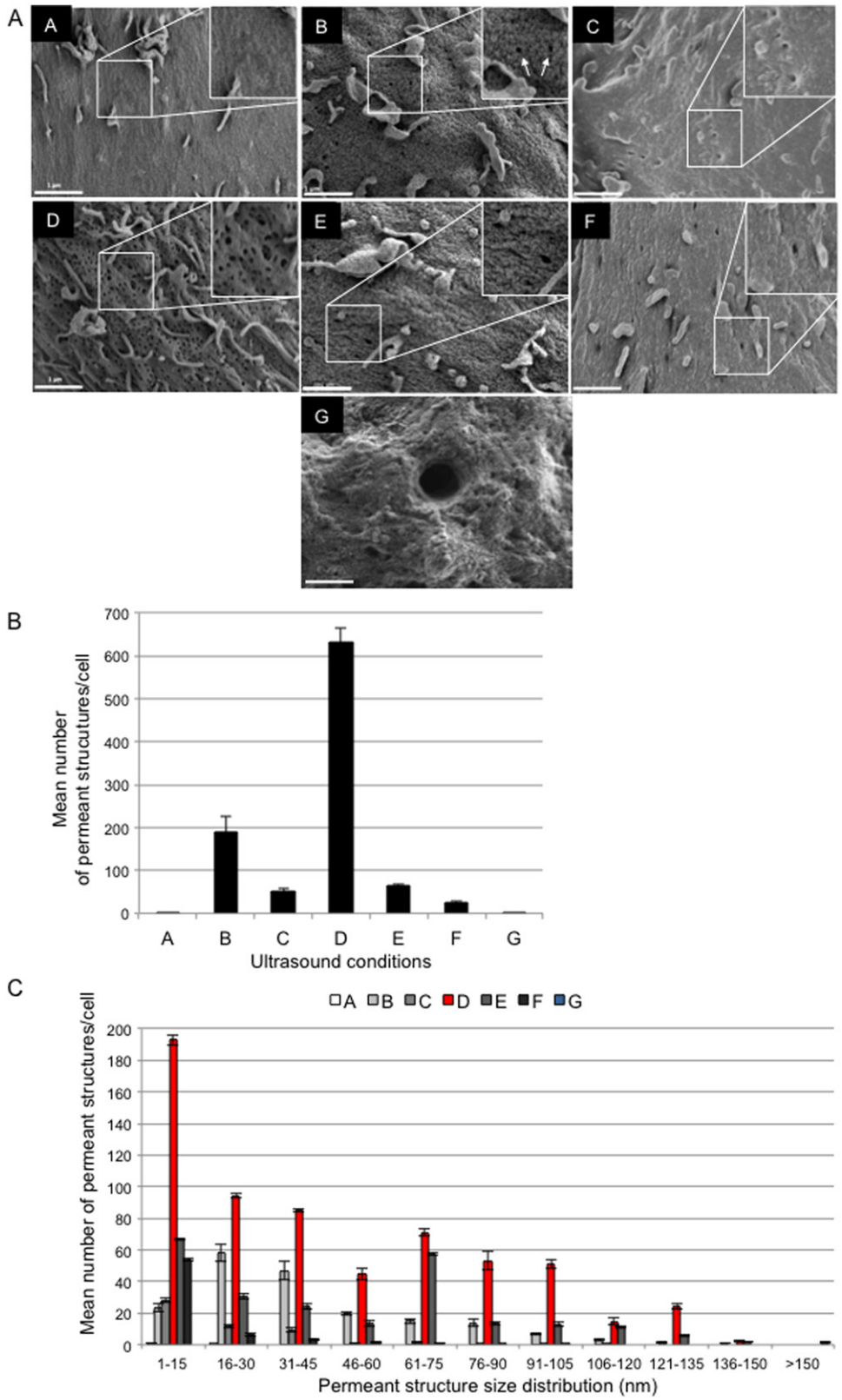

Figure 3. Ultra-structural modifications of U-87 MG cell membranes after sonoporation. U-87 MG cells were exposed to different ultrasound conditions (table 1) either in absence or in presence of microbubbles and immediately fixed after sonoporation for subsequent SEM imaging (A). The mean number (B) and size distribution (C) of the permeant structures per cells were represented (scale bar—1 μm).

endocytic invaginations or vesicles were rarely observed near the plasma membrane of control glioblastoma cells (1 $\pm$ 1 endocytic invaginations or vesicles per cell; figure 5(B)). No disruption of plasma membrane was detectable and hence was considered absent. In contrast, after sonoporation, a greater number of uncoated pits was observed at the plasma membrane level of cells (27 $\pm$ 2 versus 1 $\pm$ 1

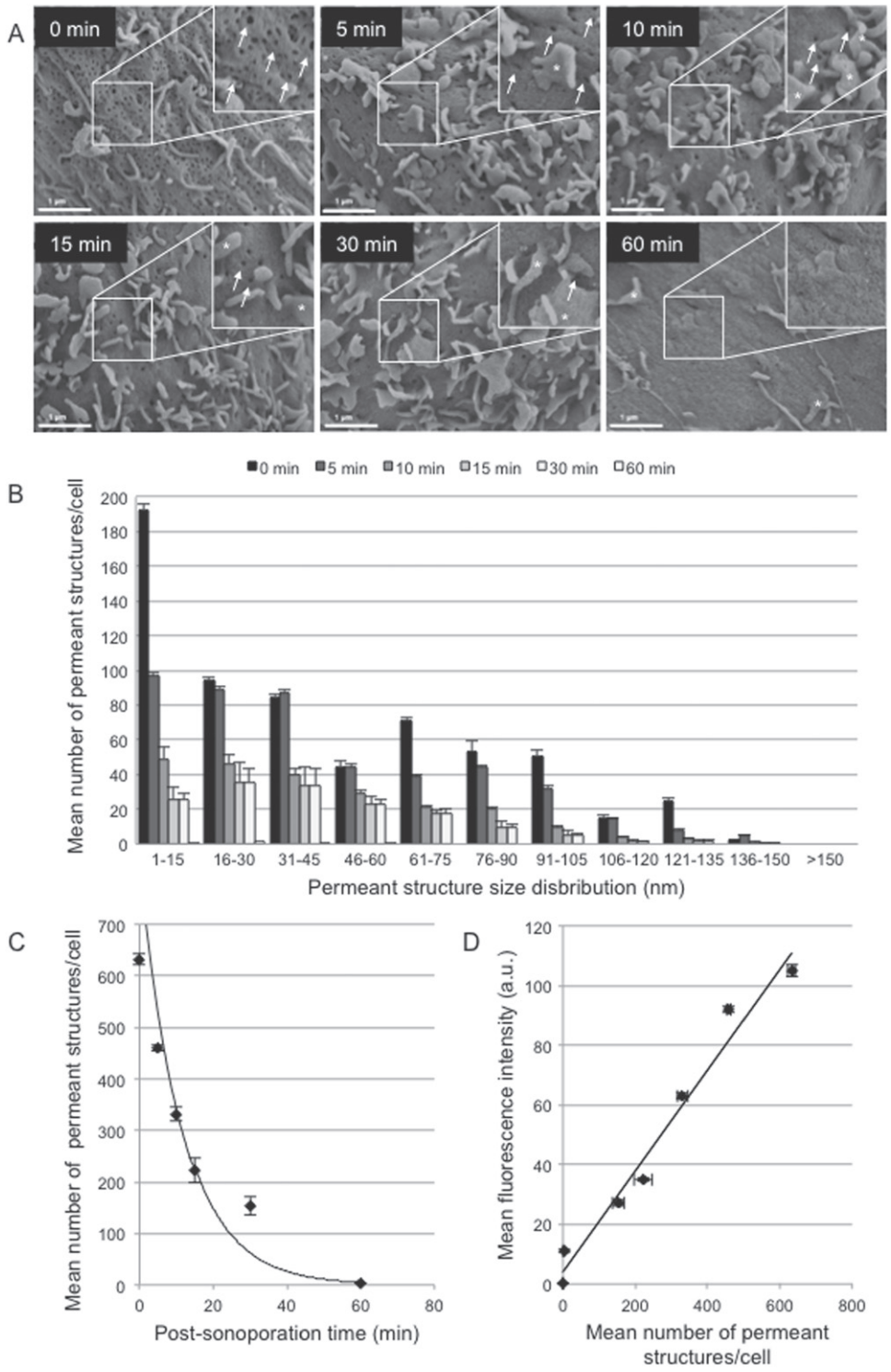

Figure 4. Evolution of permeant structures as function of time post-sonoporation. U-87 MG cells were exposed to optimal ultrasound parameters (condition D) in presence of microbubbles and immediately fixed and scanned using SEM at different time-points post-sonoporation (0–60 min) (scale bar—1 μm) (A). Size distribution of the permeant structures per cell was analyzed (B). Kinetics of permeant structure resealing (C). Mean number of permeant structures per cell was quantified as a function of time. Correlation between the mean number of permeant structures per cell and changes in membrane permeability (SYTOX-Green uptake) after sonoporation (D). The mean fluorescence intensity associated to the SYTOX-Green uptake into cells as a function of the mean number of permeant structures per cell were plotted.

uncoated pits per cell; figures 5(A) and (B)). Similarly, control (i.e., untreated) cells exhibited fewer numbers of clathrin-coated pits per cell (1 ± 1) compared to sonoporated cells (2 ± 1 clathrin-coated pits per cell; figures 5(A) and (B)). Besides, disruptions of plasma membrane were also detected in sonoporated cells (3 ± 1 membrane disruptions per cell; figures 5(A) and (B)). These observations suggest that the sonoporation probably increases the native permeability of plasma membranes to small molecules not only

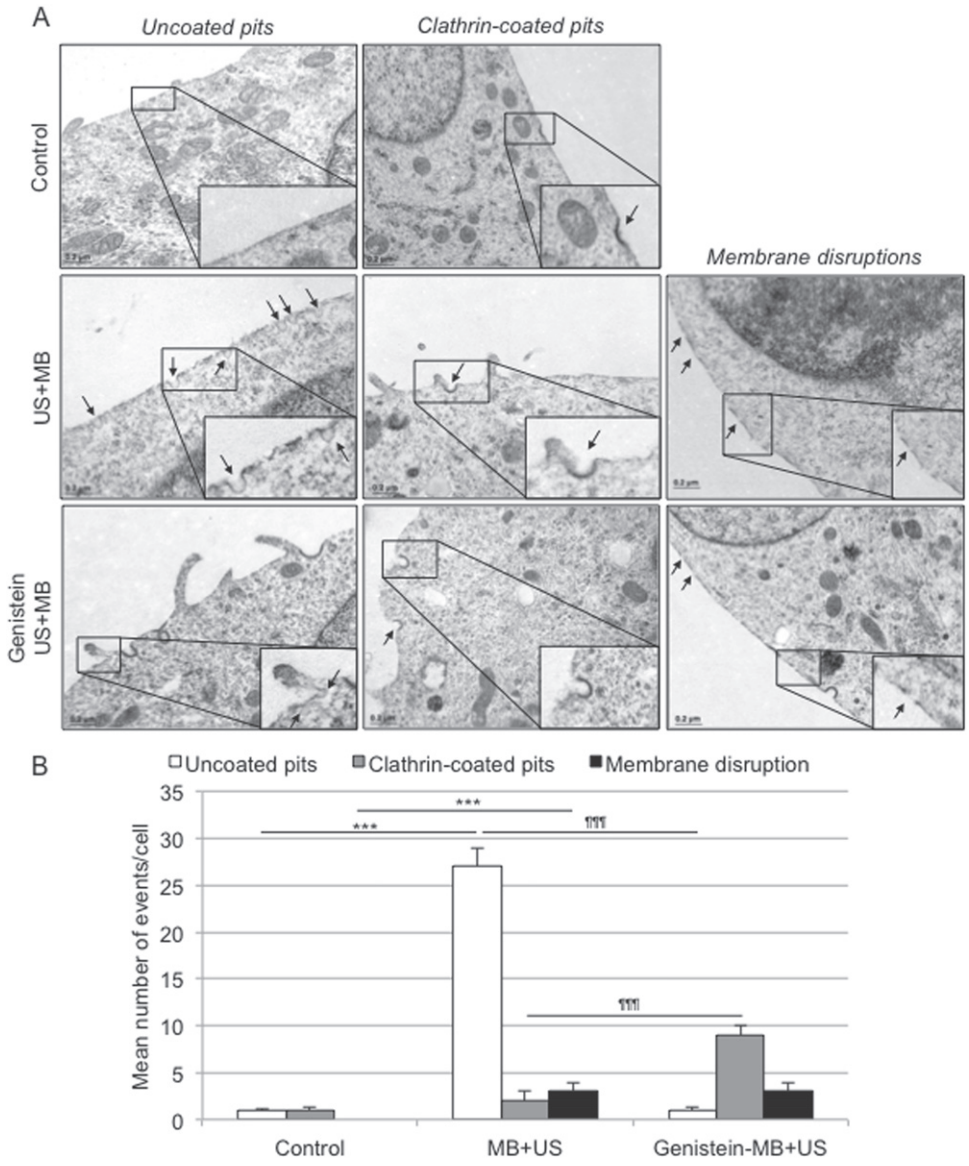

Figure 5. Identification of permeant structures by transmitted electron microscopy. Untreated and genistein-treated U-87 MG cells were immediately fixed after exposure to optimal ultrasound condition (condition D) in presence of microbubbles. They were then embedded and scanned using TEM (scale bar—0.2 μm) (A). Mean number of uncoated pits, clathrin-coated pits and membrane disruption events were quantified (B).

through membrane disruptions but also endocytosis pathways.

The uncoated pits are currently associated to the caveolae-endocytosis pathways. To determine whether or not caveolae-endocytosis pathway is involved in the sonoporation-mediated membrane permeabilization, cells were treated prior to sonoporation with genistein, an inhibitor of this pathway. The genistein-treated cells were immediately fixed after sonoporation and then embedded. TEM scans of thin-sectioned cells were subsequently acquired, in order to monitor changes in the plasma membrane (figure 5(A)). The number of uncoated pits for sonoporated cells pre-treated with genistein decreased significantly as compared to sonoporated cells without genistein incubation (1 ± 1 uncoated pits versus 27 ± 2 uncoated pits; figure 5(B)), thus confirming that sonoporation stimulated the caveolae-dependent endocytosis. Surprisingly, the mean number of clathrin-coated pits observed at the membrane level was significantly enhanced for sonoporated cells pre-treated with genistein as compared to sonoporation cells without genistein (9 ± 2 clathrin-coated pits versus 2 ± 1 clathrin-coated pits; figure 5(B)). A plausible explanation for this phenomenon is that genistein incubation probably modifies the physicochemical properties of the plasma membrane, leading to the stimulation of clathrin-mediated endocytosis. In addition, the mean number of membrane disruptions remained unchanged and their occurrence was independent of the experimental conditions (3 ± 1 membrane disruptions; figure 5(B)).

In order to confirm these findings, SEM scans of genistein-treated and sonoporated cells were acquired

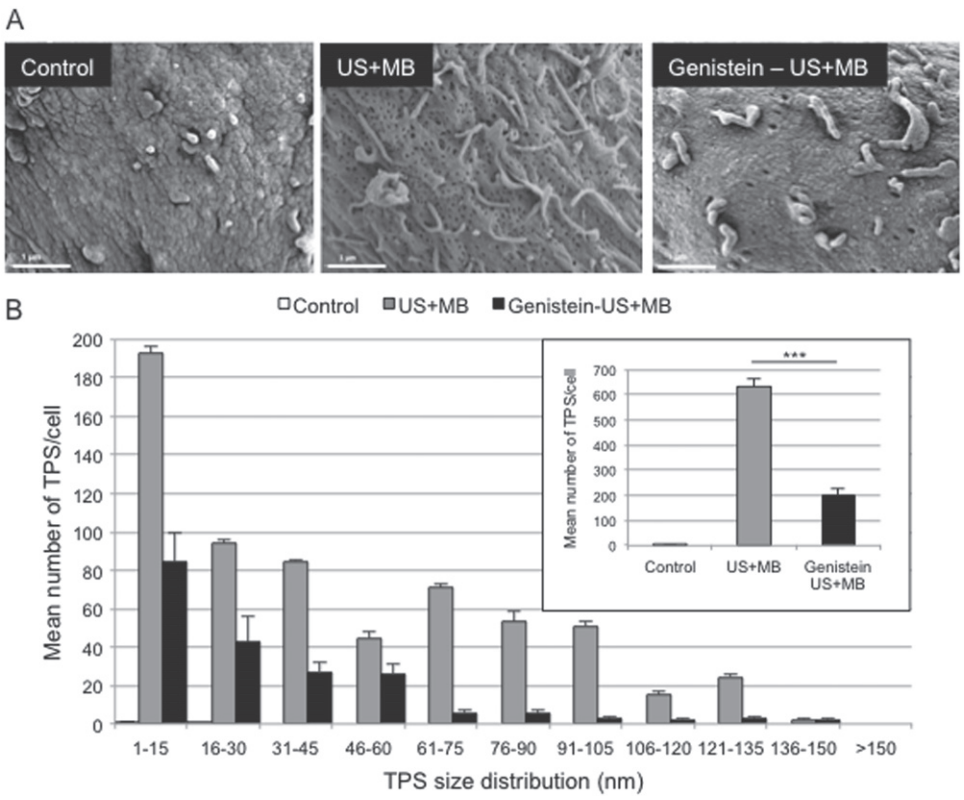

Figure 6. Sonoporation-stimulated caveolae-dependent endocytosis. Untreated and genistein-treated U-87 MG cells were immediately fixed after exposure to optimal ultrasound condition (condition D) in presence of microbubbles and subsequently scanned using SEM (scale bar—1 μm) (A). Size distribution and analysis of number ((B) *insert*) of the permeant structures (B).

and compared with SEM images of cells subjected to sonoporation alone (figure 6). Figure 6(B) shows that incubation of the cells with genistein led to a three-fold decrease in the random distribution of TPS as compared to sonoporated cells (200 $\pm$ 28 TPS versus 633 $\pm$ 32 TPS; figure 6(B), *insert*). The size distribution of these structures was similarly heterogeneous (figure 5(B)). It is worth noticing however that the mean number of these structures was similar to that observed when ultrasound was applied in the absence of microbubbles (200 $\pm$ 28 TPS versus 189 $\pm$ 39 TPS; figure 3(B)), thus confirming that the combination of microbubbles and ultrasound was central to the formation of the TPS. Moreover, the assessment of membrane permeabilization using SYTOX-Green and flow cytometry revealed that the treatment of cells with genistein led to a two-fold decrease in permeabilization level (27 $\pm$ 1% versus 59 $\pm$ 2%) and efficiency (54 $\pm$ 1 a.u. versus 105 $\pm$ 3 a.u.) as compared to the sonoporated cells without genistein incubation. In agreement with electron microscopy data, these results support the hypothesis that the caveolae-dependent endocytosis is to a large extent responsible for the membrane permeabilization and the delivery of small exogenous molecules (figure 6). Nevertheless, the involvement of clathrin-dependent endocytosis in the sonoporation process cannot be absolutely excluded. Further investigations are necessary to determine the role of this endocytic pathway in the membrane permeabilization using sonoporation.

Previous studies have mainly reported the involvement of caveolae- and clathrin-dependent endocytosis in sonoporation-mediated uptake of macromolecules such as 500 kDa dextrans [12, 32]. Unlike previous studies that were based on indirect observations, our results based on electron microscopy observations, complement previous studies, and offer visual evidences that sonoporation stimulates the endocytosis pathways and generates membrane disruptions. In addition, our data support the involvement of endocytosis, specially caveolae-mediated endocytosis, in the sonoporation-induced uptake of small molecules while most previous studies reported that small molecules and macromolecules cross the permeabilized membrane through membrane pores and endocytosis pathways, respectively [12, 32]. However, a recent real-time study described the recruitment of clathrin-mediated endocytosis in sonoporation-mediated delivery of small molecules (i.e., SYTOX-Green $\approx$600 Da) in rat C6 glioma cells [22]. The difference observed in the stimulation of endocytosis pathways (i.e., clathrin—versus caveolae—mediated endocytosis) might be due to different ultrasound parameters, microbubble and cell types used in both studies. Based on these evidences, the term of sonoporation, which suggests the formation of membrane pores only,

might be not appropriate to describe the phenomenon of acoustically-mediated membrane permeabilization. Thus, sonopermeabilization should be used to define this phenomenon. Microbubble-assisted ultrasound might improve the uptake of the small therapeutic molecules and macromolecules into the cells by stimulating the endocytosis. Thus, Lee *et al* reported that the acoustically-enhanced endocytosis of pDNA polyplexes increased gene expression. delivery using cationic lipids or polymers has been already reported [33]. In chemotherapy, microbubble-assisted ultrasound might increase the intracellular uptake of low molecular weight chemotherapeutic drugs through the stimulation of endocytotic pathways, thus enhancing the therapeutic efficiency of these compounds [34].

Perhaps most importantly, the nature of stimuli involved in increasing membrane permeability has not yet been elucidated. It has been widely proposed that the exposure of microbubbles to ultrasound causes their oscillations, which lead to intense liquid flow around the microbubble, so-called micro-streaming [4]. At even higher acoustic pressures, the microbubbles undergo large oscillations in a process leading to violent collapse and destruction of the microbubbles. This collapse might be accompanied by the generation of shock waves in the medium surrounding the microbubbles [5]. In the case of asymmetrical collapse, jet formation may also occur when a collapsing microbubble is located near a boundary such as a cell membrane [6]. As a result, these physical phenomena can generate mechanical stimuli on the plasma membrane, responsible for its permeabilization through the stimulation of endocytosis and the formation of membrane disruptions or pores. We have recently reported that microbubble destruction occurs under the same ultrasound parameters used in this study [26]. Microbubble destruction probably causes shear stress on the plasma membrane, with further stimulation of the endocytosis pathways. Electrophysiological studies demonstrated that sonoporation-mediated shear stress elicit calcium ion influx, which leads to the activation of BKCa stress-activated channels and a subsequent, local hyperpolarization of the cell membrane [15]. This hyperpolarization may facilitate uptake of exogenous molecules through endocytosis [15, 16, 35].

4. Conclusion

In summary, the present study highlights a positive correlation between the direct visualization of the ultra-structural changes in the permeabilized membrane using SEM and the assessment of membrane permeabilization by flow cytometry using SYTOX-Green. Our results show that sonoporation induces membrane permeabilization through the formation of TPS*s*. Using TEM, these structures have been identified as being caveolar endocytic vesicles.

Conflict of interest

The authors confirm that this article content has no conflicts of interest.

Author's contributions

AZ is responsible for the design of experiments and performance of all experiments. JME and AB analyze the data. JME and AB are responsible for the writing of the manuscript and the supervision of this work.

Acknowledgments

This work was supported by grants from Inserm, the ANR Soundelivery (ANR-14-CE17-0008-01) and the European Commission FP7 Program SONODRUGS (NMP4-LA-2008-213706). The authors thank Dr R Uzbekov (Microscopy Department, University F Rabelais, Tours, France) for his technical support, Professor P Roingeard (Inserm UMR 966, Tours, France), Professor C R Andres (Inserm UMR 930, Tours, France) for fruitful discussions, Dr C Sennoga (Inserm UMR 930, Tours, France) for proofreading the manuscript and Bracco Research Geneva for supplying the BR14 microbubbles.

References

[1] Delalande A *et al* 2011 Ultrasound and microbubble-assisted gene delivery in Achilles tendons: long lasting gene expression and restoration of fibromodulin KO phenotype *J. Control Release* **156** 223–30

[2] Lentacker I, Geers B, Demeester J, de Smedt S C and Sanders N N 2010 Tumor cell killing efficiency of doxorubicin loaded microbubbles after ultrasound exposure *J. Control Release* **148** e113–4

[3] Escoffre J M, Zeghimi A, Novell A and Bouakaz A 2013 *In vivo* gene delivery by sonoporation: recent progress and prospects *Curr. Gene. Ther.* **13** 2–14

[4] Doinikov A A and Bouakaz A 2010 Acoustic microstreaming around a gas bubble *J. Acoust. Soc. Am.* **127** 703–9

[5] Ohl C D and Wolfrum B 2003 Detachment and sonoporation of adherent HeLa-cells by shock wave-induced cavitation *Biochim. Biophys. Acta* **1624** 131–8

[6] Ohl C D *et al* 2006 Sonoporation from jetting cavitation bubbles *Biophys. J.* **91** 4285–95

[7] Escoffre J M, Novell A, Serriere S, Lecomte T and Bouakaz A 2013 Irinotecan delivery by microbubble-assisted ultrasound: *in vitro* validation and a pilot preclinical study *Mol. Pharm.* **10** 2667–75

[8] Park E J, Zhang Y Z, Vykhodtseva N and McDannold N 2012 Ultrasound-mediated blood–brain/blood–tumor barrier disruption improves outcomes with trastuzumab in a breast cancer brain metastasis model *J. Control Release* **163** 277–84

[9] Kotopoulis S, Dimcevski G, Gilja O H, Hoem D and Postema M 2013 Treatment of human pancreatic cancer using combined ultrasound, microbubbles, and gemcitabine: a clinical case study *Med. Phys.* **40** 072902

[10] Lammertink B, Bos C, Deckers R, Storm G, Moonen C and Escoffre J M 2015 Sonochemotherapy: from bench to bedside *Front. Pharmcol.* **6** 138

[11] Lentacker I, De Cock I, Deckers R, de Smedt S C and Moonen C T 2014 Understanding ultrasound induced sonoporation: definitions and underlying mechanisms *Adv. Drug Deliv. Rev.* **73** 49–64

[12] Meijering B D *et al* 2009 Ultrasound and microbubble-targeted delivery of macromolecules is regulated by induction of endocytosis and pore formation *Circ. Res.* **104** 679–87

[13] Mehier-Humbert S, Bettinger T, Yan F and Guy R H 2005 Plasma membrane poration induced by ultrasound exposure: implication for drug delivery *J. Control Release* **104** 213–22
[14] Derieppe M, Yudina A, Lepetit-Coiffe M, de Senneville B D, Bos C and Moonen C 2013 Real-time assessment of ultrasound-mediated drug delivery using fibered confocal fluorescence microscopy *Mol. Imaging Biol.* **15** 3–11
[15] Tran T A, Roger S, Le Guennec J Y, Tranquart F and Bouakaz A 2007 Effect of ultrasound-activated microbubbles on the cell electrophysiological properties *Ultrasound Med. Biol.* **33** 158–63
[16] Juffermans L J, Kamp O, Dijkmans P A, Visser C A and Musters R J 2008 Low-intensity ultrasound-exposed microbubbles provoke local hyperpolarization of the cell membrane via activation of BK(Ca) channels *Ultrasound Med. Biol.* **34** 502–8
[17] Yang F *et al* 2008 Experimental study on cell self-sealing during sonoporation *J. Control Release* **131** 205–10
[18] Zhong W, Sit W H, Wan J M and Yu A C 2011 Sonoporation induces apoptosis and cell cycle arrest in human promyelocytic leukemia cells *Ultrasound Med. Biol.* **37** 2149–59
[19] Zeghimi A, Novell A, Thepault R A, Vourc'h P, Bouakaz A and Escoffre J M 2014 Serum influence on *in vitro* gene delivery using microbubble-assisted ultrasound *J. Drug Target* **22** 748–60
[20] Deibert C P, Zussman B M and Engh J A 2015 Focused ultrasound with microbubbles increases temozolomide delivery in U87 transfected mice *Neurosurgery* **76** N22–3
[21] Liu H L, Huang C Y, Chen J Y, Wang H Y, Chen P Y and Wei K C 2014 Pharmacodynamic and therapeutic investigation of focused ultrasound-induced blood–brain barrier opening for enhanced temozolomide delivery in glioma treatment *PLoS One* **9** e114311
[22] Derieppe M, Rojek K, Escoffre J M, Denis de Senneville B, Moonen C and Bos C 2015 Recruitment of endocytosis in sonopermeabilization-mediated drug delivery: a real-time study *Phys. Biol.* **12** 046010
[23] Vercauteren D *et al* 2010 The use of inhibitors to study endocytic pathways of gene carriers: optimization and pitfalls *Mol. Ther.* **18** 561–9
[24] Li Y S, Davidson E, Reid C N and McHale A P 2009 Optimising ultrasound-mediated gene transfer (sonoporation) *in vitro* and prolonged expression of a transgene *in vivo*: potential applications for gene therapy of cancer *Cancer Lett.* **273** 62–9
[25] Qiu Y *et al* 2010 The correlation between acoustic cavitation and sonoporation involved in ultrasound-mediated DNA transfection with polyethylenimine (PEI) *in vitro J. Control Release* **145** 40–8
[26] Escoffre J M, Novell A, Piron J, Zeghimi A, Doinikov A and Bouakaz A 2013 Microbubble attenuation and destruction: Are they involved in sonoporation efficiency? *IEEE Trans. Ultrason. Ferroelectr. Freq. Control* **60** 46–52
[27] van Wamel A *et al* 2006 Vibrating microbubbles poking individual cells: drug transfer into cells via sonoporation *J. Control Release* **112** 149–55
[28] Duvshani-Eshet M, Baruch L, Kesselman E, Shimoni E and Machluf M 2006 Therapeutic ultrasound-mediated DNA to cell and nucleus: bioeffects revealed by confocal and atomic force microscopy *Gene Ther.* **13** 163–72
[29] Yudina A, Lepetit-Coiffe M and Moonen C T 2011 Evaluation of the temporal window for drug delivery following ultrasound-mediated membrane permeability enhancement *Mol. Imaging. Biol.* **13** 239–49
[30] Lammertink B, Deckers R, Storm G, Moonen C and Bos C 2015 Duration of ultrasound-mediated enhanced plasma membrane permeability *Int. J. Pharm.* **482** 92–8
[31] Zhou Y, Shi J, Cui J and Deng C X 2008 Effects of extracellular calcium on cell membrane resealing in sonoporation *J. Control Release* **126** 34–43
[32] Afadzi M *et al* 2013 Mechanisms of the ultrasound-mediated intracellular delivery of liposomes and dextrans *IEEE Trans. Ultrason. Ferroelectr. Freq. Control* **60** 21–33
[33] Lee J L, Lo C W, Inserra C, Bera J C and Chen W S 2014 Ultrasound enhanced PEI-mediated gene delivery through increasing the intracellular calcium level and PKC-delta protein expression *Pharm. Res.* **31** 2354–66
[34] Tardoski S, Gineyts E, Ngo J, Kocot A, Clezardin P and Melodelima D 2015 Low-intensity ultrasound promotes clathrin-dependent endocytosis for drug penetration into tumor cells *Ultrasound Med. Biol.* **41** 2740–54
[35] Tran T A, Le Guennec J Y, Bougnoux P, Tranquart F and Bouakaz A 2008 Characterization of cell membrane response to ultrasound activated microbubbles *IEEE Trans. Ultrason. Ferroelectr. Freq. Control* **55** 43–9